DOI: 1061294/jiaps2023.2736 ISSN 0974 - 9373

Vol. 27 No. 3 (2023) **J. Int. Acad. Phys. Sci.** pp. 259-274

Analysis of volume fraction of Casson Nanofluid flow over a flat moving plate with thermal radiation and nonuniform heat source/sink

Jagadish V Tawade*
Vishwakarma University, Kondhwa (BK), Pune-411048, Maharashtra, India
Corresponding author Email: jagadish.tawade@vupune.ac.in

Mahadev M Biradar
Department of Mathematics, Basavesvara Engineering College, Bagalkot-587102, Karnataka, INDIA
Email: mmbbec@gmail.com

Dakshayini N
Department of Mathematics, Visvesvaraya Technological University, Belagavi-590018, Karnataka, INDIA
Email: dakshayini6@gmail.com

Manjunatha B
Government First Grade College for Women Jevargi Colony, Gulbarga-585102

(Received March 24, 2023, Accepted June 18, 2023)

Abstract: We provide numerary analysis of Casson nanofluids flowing through porous materials on stretched magnetic surfaces. The behavior of non-Newtonian liquids is described by the Casson liquid model. Similarity transformations are used to create nonlinear partial differential equations and are solved using numerical methods. Nusselt Number, Skin Friction Coefficient, Temperature, Velocity results are collected. Graphs are used to show the effects of physical factors on the flow and heat transfer properties of nanofluids. These include the Kasson parameter, the porosity parameter, the magnetic parameter, the radiation parameter, and the Prandtl number. Results show that the temperature profile increases while the velocity field decreases with increasing Casson nanofluidic parameters. A decrease in the thickness of the pulse boundary layer and an increase in the thickness of the thermal boundary layer can be seen with increasing magnetic parameters alone.

Keywords: MHD, Casson nanofluid parameter, Stretching sheet, Permeability/porous medium.

1. Introduction

The purpose of the work of Al Mamun *et al.*[1] is to explain the flow of non-Newton-Casson fluids by mass and heat conduction to elongated surfaces coupled with periodic hydromagnetic effects, along with the effects of thermophoresis and radiation absorption. In this case, the endothermic parameters are also included. A time-dependent set of linear equations was established to describe the fluid flow system, including momentum, energy, and concentration. The purpose of Aisha *et al.*[2] is to understand the heat transfer and mhd boundary layer flow of non-Newtonian fluids across stretched surfaces in porous media. The behavior of non-Newtonian liquids is described by his Casson liquid model. Two different forms of nanofluids are being investigated, Cu-water and Ag-water. Bagh *et.al.*[3,4] have investigated the dual Christophe-Cattaneo dispersion and activation energies in the unstable magnetohydrodynamic transitions of rotating Maxwellian nanofluidic flows across stretched foils. The Arrhenius activation energy is used to assess the dispersion of chemically reactive species. In this paper, we describe how rotating water-based silver nanoparticles direction of a continuous stretched film, considering the effects of volume fraction, Coriolis force and Lorentz force. By influencing the fluid motion on the Earth's surface, the Coriolis force has a significant impact on fluid dynamics in material study, solar dynamics, marine, and astronomy. The inclusion of nanoparticles is due to certain properties, including improved heat transfer, and is important in heat exchanger, advanced nanotechnology, electronics, and materials science. Improving heat transport is the main goal of this work.

Current research focuses on incompressible and conductive biomagneto-hydrodynamic (BFD) flow[5], specifically blood flow containing magnetic particles through a cylinder that is stretched in two dimensions under the action of a magnetic dipole.are investigating. Here, the relationship between liquid viscosity and thermal conductivity is assumed to be reciprocal, and the relationship with temperature is assumed to be linear. Two analytical subfields-strong hydrodynamics (FHD) and magnetohydro-dynamics (MHD) - are involved in this investigation (FHD). We describe the basic properties of pure blood and the properties that emerge when magnetic particles are introduced into the blood. The outcome shows that the velocity of the liquid (blood-Fe_3O_4) declines with increasing values of the other ferromagnetic interaction parameters, while the curvature parameters axial velocity and temperature increase. Both the heat transfer coefficient and the skin friction coefficient decrease as the value of the thermal conductivity parameter increases. The study also included a stability analysis over time to ensure the results were physically reliable. In their work, Gadicolaei *et al*.[6] investigated and performed numerical analysis of MHD flow-mixing convection in Casson nanofluids across nonlinear permeable stretch sheets. Consider how heat is generated or absorbed by thermal radiation, chemical reactions, viscous dissipation, suction, and Joule heating. Nanoparticles are modeled using Brownian motion and thermophoretic phenomena (Buongiorno's model). In the work of Gnaneswara *et al*.[7], the problem of laminar boundary laminar flow and heat transfer in MHD fluids induced by unstable stretched films with extended heat flow is considered. Thermal conductivity and viscosity are thought to vary with temperature. In the work, Hamze *et al*.[8] used magnetic fields to investigate heat transfer in Casson hybrid nanofluids across vertically stretched foils. Methanol contains copper oxide and graphite oxide, which are considered hybrid nanoparticles. The studies in this study shed light on various physical properties of flow related to heat transfer.

Ibrah *et al*.[9] investigated the effects of thermally radiating magneto-nano-casson liquids on fine needles. Navier used his slip effect to simulate the problem numerically. MWCNTs, also called multi-walled carbon nanotubes, reduce friction. Compared to parabolic rotation, the surface of the needle transfers heat faster from the liquid. Compared to single-walled carbon nanotubes, multi-walled carbon nanotubes transport more heat from fluids (SWCNTs). SWCNTs are superior to MWCNTs in terms of heat transfer because paraboloids conduct heat more efficiently than cylindrical surfaces. Kamran *et al*.[10] performed a numerical analysis of Casson nanofluids on a horizontally spreading surface under the influence of magnetism. The analysis considers the slip boundary condition and the thermal convection boundary condition. Kouse *et al*.[11] investigated the heat transfer properties of non-Newtonian Casson nanofluids and their three-dimensional flow across a linearly extending plane in a rotating frame. Buongiorno's nanofluidic model included in the current model involves thermal transfer and random motion of nanoparticles. Both continuous heat flow and viscous heating mechanisms at the boundary were also considered. In the article, Liaquat *et al*[12]. used magnetohydrodynamics (MHD) theory to study the flow of Casson nanofluids with thermal radiation across unstable contracting surfaces. For the Navier-Stokes design of a non-Newtonian fluid with symmetric elements in the viscosity term, a momentum equation is obtained. We also consider how a Stephan bubble with velocity, concentration, and temperature partial slip conditions affects the velocity, concentration, and temperature distributions.

The purpose of the article[13] is to study the effects of heat generation and coalescence on the boundary-level flow of viscous liquids induced by unevenly stretched sections in the absorbing medium with changes in external heat. Numerical solutions of the same equations are obtained by a shooting procedure to obtain analogous solutions of the modified main equations. A detailed investigation and analysis is carried out on the current and heat transfer characteristics for various dates of relevant factors. In current research[14], gradient magnetic fields, viscous dissipation, and radiation are used as non-uniform heat sources/sinks and chemical reactions. Various types of nanoparticles were examined in this study, including silver, copper, aluminum oxide, titanium oxide, and magnesium oxide (MgO). The article of Mohammed *et al.*[15] provides a computational analysis of the effects of nonlinear thermal radiation, heat generation/absorption, Joule heating, and slip limit conditions on the magnetohydrodynamic flow of Casson nanofluids across stretched sheets through porous materials increase. The nanofluidic combination is modeled using a two-phase nanofluidic approach. The Darcy model serves as a representation of porous materials. Muradi *et al.*[16] conducted on magnetohydrodynamically unstable Sakiadis and Blasius boundary layer flows in nanofluids with leading edge accretion/ablation explore the combined effects of bioconvection and magnetic fields. In addition, we were able to investigate the effects of Biot number, thermal radiation, chemical reactions and convective boundary conditions. The magnetization is acting transverse to the plate and is constant, and convective conditions and radiant heat sources exist at the boundary. The goal of the study[17] is to study how two immiscible thin liquid films flow across a linearly expanding foil in the presence of a uniform transverse magnetic field. The aim of the study[18] is to study the effects or consequences of the heat source parameter via a wedge across the porous medium on the conductive fluid flow of magnetohydrodynamic Casson nanofluids with activation energy. For conducting fluids, we also investigated the effect of "second law" analysis on chemical reactions. in the work of Rafique *et al.*[19], the results of boundary layer flow with her Casson nanofluids on inclined surfaces are investigated with Soret and Dufour. His Buongiornopattern of the heat efficiency of liquid flow in the existence of Brownian motion and thermophoretic characteristics served as the basis for the model used in this study. Given the dominant flow properties of the enhanced boundary layer, we model Casson nanofluidic flow problems along inclined channels to learn more about heat and mass transfer phenomena. In the study, Ramudu *et al.*[20] investigated the heat transfer properties of a continuous two-dimensional magnetohydrodynamic shear-thickening Casson fluid across a vertically extending sheet with varying heat sources/sinks. The temperature distribution is improved by increasing the Biot number and thermal radiation parameters. It can be seen that both the distribution velocity and the temperature in the intake and injection situations decrease as the intake/injection parameters increase. In the work, Reddy *et al.*[21] investigated the effect of radiant energy on the imbalenced 3-dimensional mhd flow of a microliquid along the horizontal plane of a parabola of rotation. The work of Shiva *et.al.*[22] investigated heat and mass transport in unstable two-dimensional Casson nanofluidic flows through porous sheets stretched nonlinearly with respect to chemical reactions, viscous dissipation, heat emission, and radiant energy. The equations governing the boundary layer are made dimensionless before being solved using the explicit finite difference method. Effective convergence criteria are determined using stability analysis. This makes the numerical method more reliable. To investigate the implications of various flow parameters, profiles of temperature, velocity and nanoparticle concentration are shown. The article's goal[23] is to investigate the combined effects of suction/injection, external magnetic fields, and 1st order binding processes on the forced convective motion of nanoliquids over absorbent sheets. Zero nanoparticle flux at the boundary is postulated to push components still on the plate surface to control the flux. As a result, the model can be used in various engineering fields to passively control nanoelement components. In the work[24], the effects of synchronous magnetic fields on Williamson nanofluids on stretched surfaces with convective boundary conditions are numerically investigated. With Christophe-Cattaneo double diffusion on stretched surfaces, the work[25] intends to examine the heat and mass transmission of Williamson mhd nanofluids in porous media. Additionally, we investigate the impacts of chemical processes, radiation, heat production, and sucking/injecting effects on current flow. We found that the decrease in the velocity field is due to the increase in the magnetic field, the porosity parameter and the attraction parameter. Furthermore, as thermal radiation raises, the heat transfer coefficient declines, On the other hand, with higher values, thermophoresis, Brownian motion, heat production, concentration, and thermal relaxation time all rise.

2. Problem Formulation

In this research, the constant 2Dmhd flow of a conducting non-Newtonian Casson nano liquid across a stretched foil at $y = 0$ is considered, along with the effects of heat generation and absorption due to chemical reactions and thermal radiation increase. In the zone where $y > 0$, the flow is contained. Applying two equal and opposite pressures along the x-axis causes the wall to expand while the origin remains stationary. The isotropic incompressible flow of Casson nanofluids is described by the rheological equation of state.

(1) $$\tau_{ij} = \left[\begin{cases} 2\left(\mu_B + \frac{P_y}{\sqrt{2\pi}}\right) e_{ij}, & \pi > \pi_c \\ 2\left(\mu_B + \frac{P_y}{\sqrt{2\pi}}\right) e_{ij}, & \pi < \pi_c \end{cases}\right]$$

$\pi = e_{ij}e_{ij}$, and e_{ij} is the $[i,\ j]^{th}$ component of deformation rate, In the non-Newtonian model, n is the product of the strain rates with itself, c is the product's critical value, B is the non-Newtonian fluid's elastic dynamic viscosity, and Py is the fluid's yield stress. Such a flow is governed by the momentum, continuity,and energy equations, whereby

(2) $$\frac{\partial u}{\partial x} + \frac{\partial v}{\partial y} = 0$$

(3) $$u\frac{\partial u}{\partial x} + v\frac{\partial v}{\partial y} = \nu_{nf}\left(1 + \frac{1}{\gamma}\right)\frac{\partial^2 u}{\partial y^2} - \left(\frac{\sigma {B_0}^2}{\rho_{nf}} + \frac{\nu_{nf}}{k_0}\right)u$$

(4) $$u\frac{\partial T}{\partial x} + v\frac{\partial T}{\partial y} = \alpha_{nf}\frac{\partial^2 T}{\partial y^2} + \frac{16\sigma^* {T_0}^3}{3\rho C_p k^*}\frac{\partial^2 T}{\partial y^2} + \frac{q'''}{\rho C_p} + \frac{Q_0}{\rho C_P}(T - T_\infty) + \frac{k u_w}{x v}$$

In the above equation, *x* & *y* direction velocity components are denoted with *u* & *v*. The Casson fluid density is ρ_{nf} and ν_{nf} is the kinematic viscosity. $\gamma = \mu_B\sqrt{\frac{2\pi_c}{P_y}}$ is the parameter of Casson, k_0 is the permeability of the medium, *T* is the temperature, Q_0 is the dimensional thermal generation/absorption coefficient, *T* is the temperature, C_p is the specific heat, α_{nf} is the thermal diffusivity.

Equation (4)'s q''' non-uniform heat source/ heat sink is represented as,

(5) $$q''' = \frac{k u_w(x)}{x v}\{A^*[T_s - T_0]f' + [T - T_0]B^*\}$$

where A^* and B^* are, respectively, the coefficients of a heat source or sink that is dependent on temperature and space. Here, we remark that the situation relates to the production of internal heat and the absorption of internal heat. Additionally, it is believed that the generated magnetic field is minuscule.

The boundary conditions affect the governing equations.

(6) $$\begin{gathered} T = T_w = T_\infty + A\left(\frac{x}{l}\right)^2 \quad at \quad y = 0 \\ u = u_w(x) = bx, \quad v = 0, \\ u \to 0, \quad T \to T_\infty \quad as\ \ y \to \infty \end{gathered}$$

where $u_w = bx, \quad b > 0$ stretching sheet velocity, *l* is Characteristic length, *A* is a constant, temperature of the foil Tw, free stream temperature T_∞, temperature of the fluid is T.

We present the subsequent similarity variables:

$$\eta = \sqrt{\frac{b}{\nu_f}}\,y$$

(7) $$\psi = x\sqrt{b\nu}f(\eta),\ \ \theta(\eta) = \left[\frac{T-T_\infty}{T_w-T_\infty}\right],$$

Where ψstream function is defined as follows in the standard fashion:

$$u = \frac{\partial\psi}{\partial y}\text{and}v = -\frac{\partial\psi}{\partial x}.$$

3. Solution Methodology

The ordinary differential equations with the following boundary conditions are eventually produced by substituting equations (6) and (7) in the PDE (3) and (4).

(8) $$f'''\left(1+\frac{1}{\gamma}\right) + \left(ff'' - f'^2 - \frac{M}{\phi_2}f'\right)\phi_1 - kf' = 0$$

(9) $$\left(1+\frac{4}{3}\ \mathrm{Tr}\right)\theta'' + \left(\frac{k_f}{k_{nf}}\mathrm{Pr}\phi_3\right)f\theta' + \mathrm{Pr}\delta\theta + \frac{\mathrm{Pr}}{k_0} + \{A^*f' + B^*\theta\} = 0.$$

Circumstances in equation (6) became.

$$f' = 1,\qquad f = 0,\quad \theta = 1\ \ at\qquad \eta \to 0$$

(10) $$f' \to 0,\ \theta \to 0\quad as\qquad \eta \to \infty$$

The following definitions apply to the dimensionless variables and integers in the equations above: M stands for the magnetic parameter, γ- Casson nanofluid parameter, and porous parameter k.

The nanoparticle volume fraction is parameter ϕ, and the Prandtl number is defined as $\frac{\nu_f}{\alpha_f}$.

The physical quantities of interest are the skin friction coefficient C_f and the local Nusselt number Nu_x, which are represented as

(11) $$C_f = \frac{\tau_w}{\rho_f {u_w}^2}\quad\text{and}\quad Nu_x = \frac{xq_w}{k(T_w-T_\infty)},$$

where τ_w is the shear stress along the strain plane, q_w is surface heat flux, both are presented as

(12) $$\tau_w = \left[\mu_B + \frac{P_y}{\sqrt{2\pi_c}}\right]\left(\frac{\partial u}{\partial y}\right)_{y=0}\ \text{and}\ \ q_w = -k\left(\frac{\partial T}{\partial y}\right)_{y=0}$$

Equations (10) and (11) are changed by substituting the transformations from (6). The result is

$$Re_x^{\frac{1}{2}} C_f = \left(1 + \frac{1}{\gamma}\right) f''(0), \quad and Re_x^{-\frac{1}{2}} Nu_x = -\theta'(0) \tag{13}$$

where $Re_x = \frac{{u_w}^2}{\nu}$ is the local Reynolds number.

4. Results Discussion

The current work investigates the research of Casson nanofluidic flow with non-uniform thermal source/sink along with viscous dissipation in the existence of mhd. Numerical calculations were performed to determine the temperature profile, velocity profile, local Nusselt number and skin friction coefficient for different values of the parameters that characterize the flow properties. This section's goal is to look at the physical implications of various implantation settings on the temperature and velocity profiles [f(η), θ(η)] displayed in graphs 1 through 15.

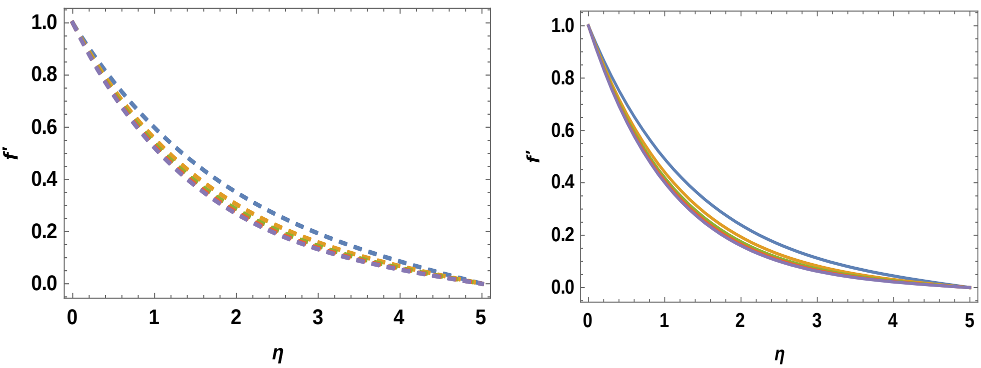

(A) (B)

Graph 1 (A & B). The effect of Casson fluid parameter $\boldsymbol{\gamma}$ onVelocity profile $\boldsymbol{f'(\eta)}$
M =1, ϕ1, ϕ2, ϕ3=0.005, 0.01, 0.03. k =0.5, kf =0.613, knf =1.08, Pr=6.2, **A***=1, **B***=1, Ec =1

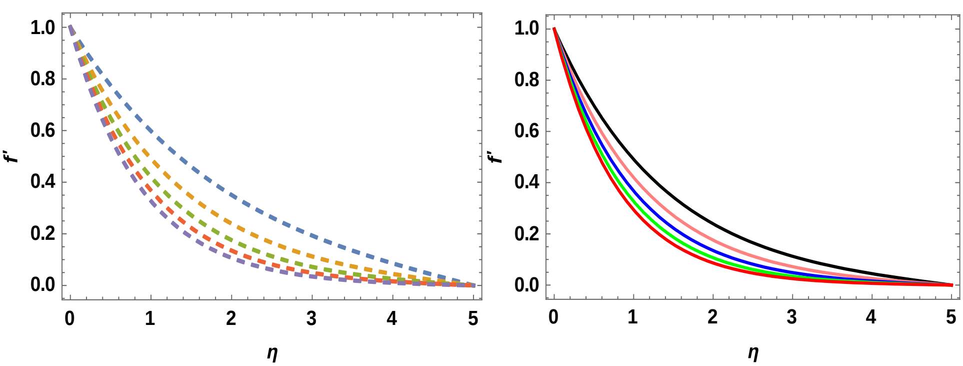

(A) (B)

Graph 2 (A & B) Velocity profile $\mathbf{f'(\eta)}$ for various values of Magnetic Parameter **M**, $\boldsymbol{\gamma}$ =1,ϕ1, ϕ2, ϕ3=0.005, 0.01, 0.03. k=0.5, k_f=0.613, k_{nf}=1.08, Pr=6.2, **A***=1, **B***=1, *Ec* =1

Graphs 1-3 show the effects of M, γ, K & f' on the velocity profile. According to Graph 1, increasing γ decreases yield stress, which in turn causes a rise in the Casson parameter, which reduces fluid plasticity. This is because increasing γ has an inverse relationship with yield stress, which causes the fluid velocity to decline for larger values of γ. The effect of M on fluid velocity is shown in Graph 2, and as would be predicted, greater numbers of M result in a decrease in fluid velocity. The cause of this behavior is that the applied magnetic field induces a resistive force in the conducting liquid, known as the Lorentz force, which equates to the resistive force.

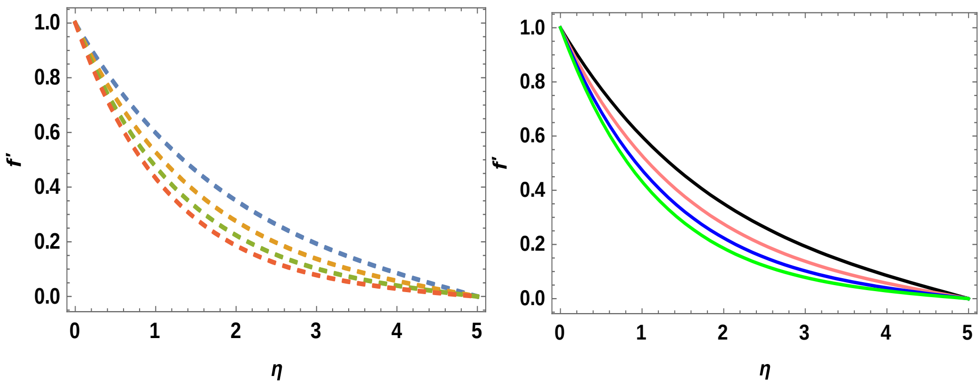

(A) (B)

Graph 3 (A & B). Velocity profile $\mathbf{f'(\eta)}$ for various values of Porosity Parameter **k**, $\boldsymbol{\gamma}$ =1, $\phi 1$, $\phi 2$, $\phi 3$=0.005, 0.01,0.03. M=1, k_f=0.613, k_{nf}=1.08, Pr=6.2, $\mathbf{A}^*$=1, $\mathbf{B}^*$=1, Ec =1

The fluid flow over the border zone is slowed down by this force. It can be shown in Graph 3 that, as k increases, the fluid velocity decelerates rapidly around stretched sheets. This physically demonstrates that the fluid's velocity next to the foil is lower compare to velocity of a stretched foil as a whole.

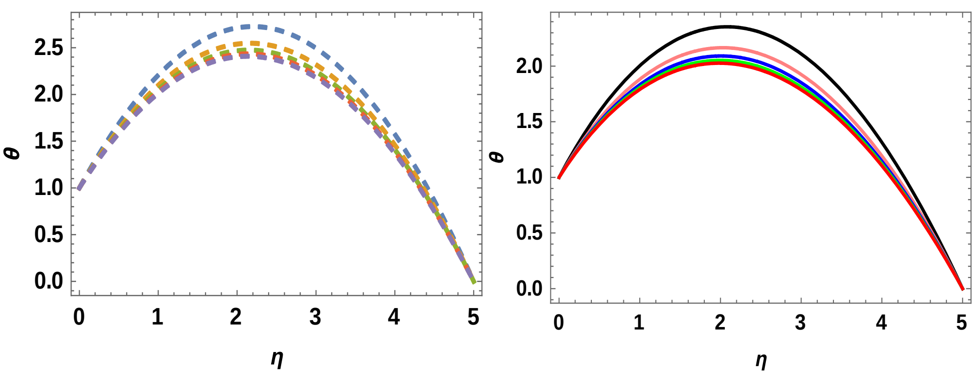

(A) (B)

Graph 4 (A & B) Temperature profile $\boldsymbol{\theta(\eta)}$ for various values of Casson Parameter $\boldsymbol{\gamma}$, M =1, $\phi 1$, $\phi 2$, $\phi 3$=0.005, 0.01, 0.03. k=0.5, k_f=0.613, k_{nf}=1.08, Pr=6.2, $\mathbf{A}^*$=1, $\mathbf{B}^*$=1, Ec =1, Nr=1

The domination of the Casson parameter γ on the temperature profile θ(η) is shown in graph 4. It is clear that when the Casson nanofluid param γ is increased, the temperature of the nanofluids rises, increasing the thickness of the thermal boundary layer as the elasticity stress parameter rises.

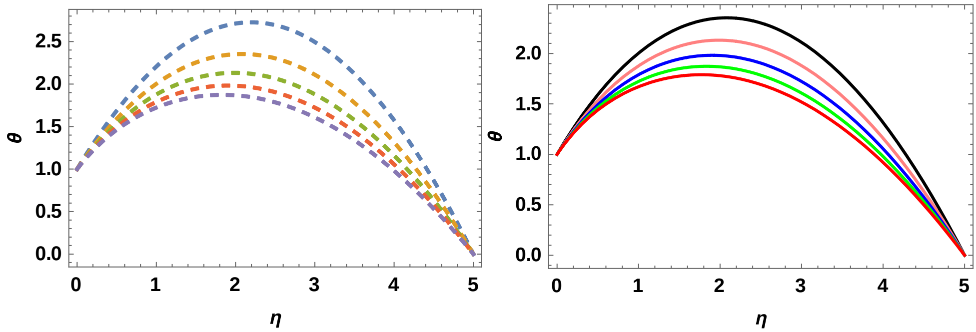

(A) (B)

Graph 5 (A & B) Temperature profile **θ(η)** for various values of Magnetic Parameter **M**, $\boldsymbol{\gamma}$=1, ϕ1, ϕ2, ϕ3=0.005, 0.01, 0.03. M=1, k_f=0.613, k_{nf}=1.08, Pr=6.2, $\mathbf{A}^*$=1, $\mathbf{B}^*$=1, *Ec* =1, Nr=1

It is clear from Graph 5 as the magnetic parameter *M* increases, the thickness of the thermal boundary layer increases as well, because the presence of the magnetic field increases the temperature of the fluid in the boundary layer. One explanation for this behavior is that when an electric current is passed through a flowing fluid, it cools down and increases the thickness of the thermal boundary layer.

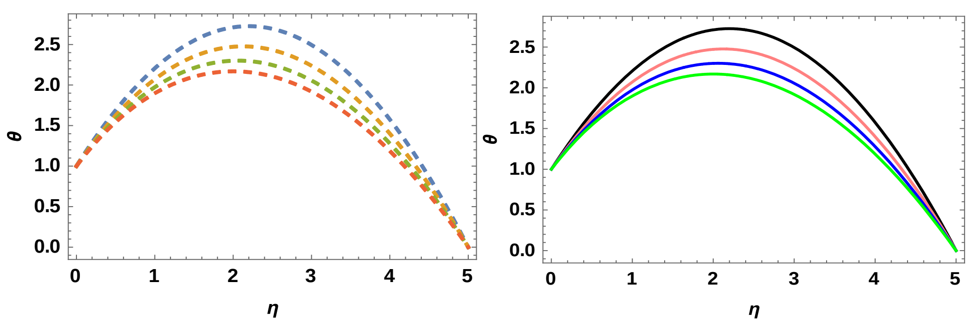

(A) (B)

Graph 6 (A & B) Temperature profile **θ(η)** for various values of Porosity Parameter **k**, $\boldsymbol{\gamma}$=1, ϕ1, ϕ2, ϕ3=0.005, 0.01, 0.03. M=1, k_f=0.613, k_{nf}=1.08, Pr=6.2, $\mathbf{A}^*$=1, $\mathbf{B}^*$=1, *Ec* =1, Nr=1

From Graph 6, it can be seen that the porous param k has an impact on the temperature diagram and that the temperature of the fluid rises as the porosity parameter's value increases. According to Graph 7, as the volume fraction of nanoparticles ϕ increases, the fluid temperature increases. The impact of Pr on the variation of temperature is seen in Graph 8. A drop in temperature profile is produced by an increase in Pr.

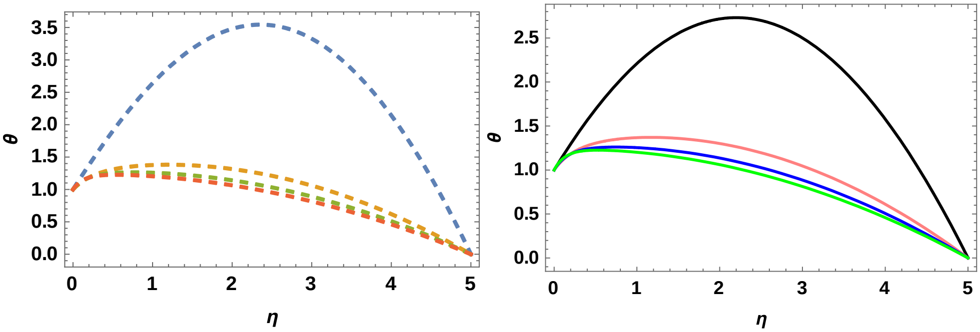

(A) (B)

Graph 7 (A & B) Temperature profile $\theta(\eta)$ for various values of nanoparticle parameter ϕ_1, γ =1,M=1,ϕ1, ϕ2=0.005, 0.01,k =0.5, k_f=0.613,k_{nf}=1.08, Pr=6.2, A^*=1, B^*=1, Ec =1, Nr=1

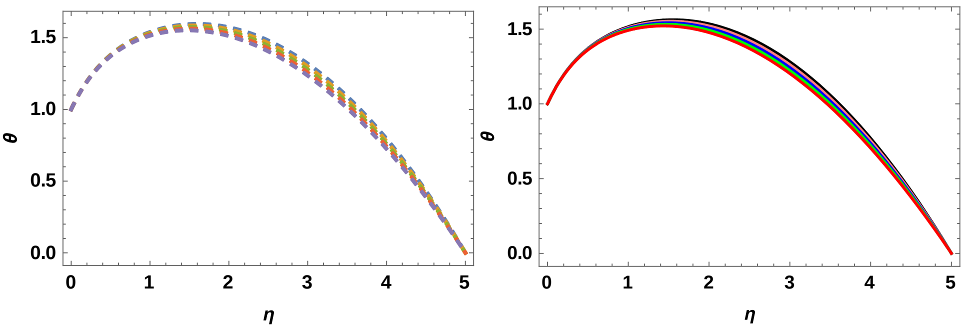

(A) (B)

Graph 8 (A & B) Temperature profile θ(η) for various values of Prandtl number Pr, γ =1, ϕ1, ϕ2, ϕ3=0.005, 0.01, 0.03. k=0.5, k_f=0.613, k_{nf}=1.08, Ec=1, A^*=1, B^*=1, M =1, Nr=1

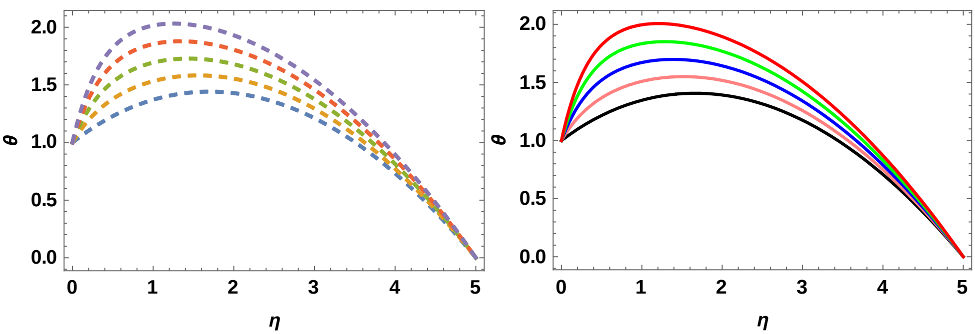

(A) (B)

Graph 9 (A & B) Temperature profile θ(η) for various values of Eckert number Ec, γ =1,ϕ1, ϕ2, ϕ3=0.005, 0.01, 0.03. k=0.5, k_f=0.613, k_{nf}=1.08, Pr=6.2, A^*=1, B^*=1, M =1, Nr=1

It may be shown from Graph 9 that raising Eckert number Ec raises the fluid temperature. Rising values of A* and B* clearly show that the variation of temperature in the border zone is increased. The non-uniform heat source/sink parameter typically has positive values that act as heat generators and negative values that act as heat absorbers from the boundary layer.

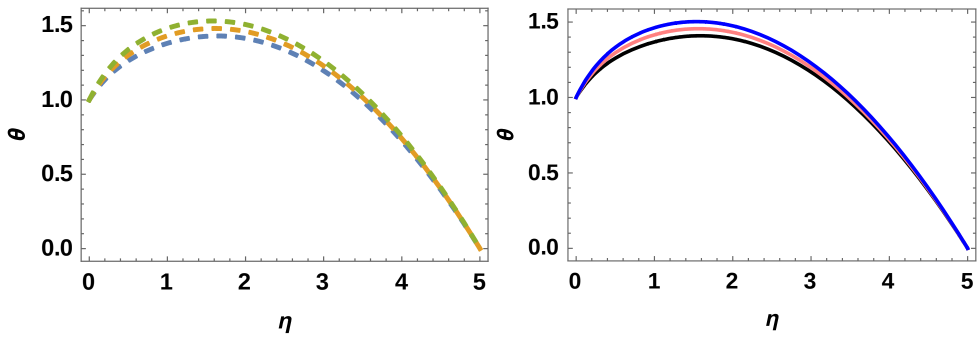

Graph 10 (A & B) Velocity profile $\theta(\eta)$ for various values of **A***, γ =1, M=1,ϕ1**,** ϕ2**,** ϕ3=0.005**,**0.01,0.03.k=0.5, k_f=0.613, k_{nf}=1.08, Pr=6.2, A*=1, *Ec*=1, Nr=1

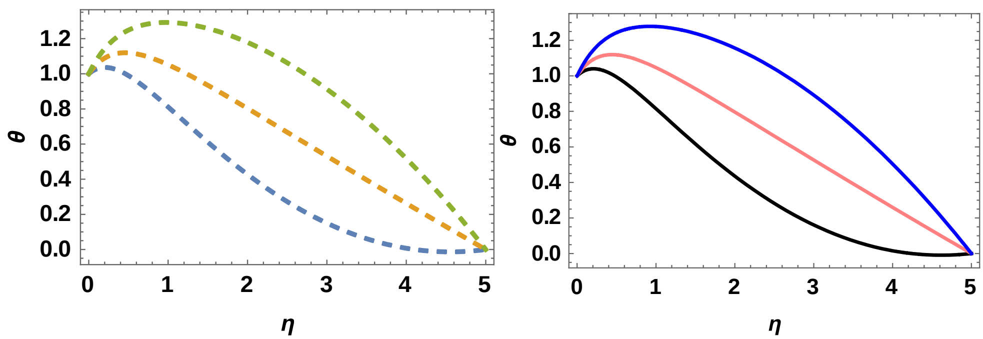

Graph 11 (A & B) Temperature profile $\theta(\eta)$ for various values of B*, $\boldsymbol{\gamma}$ =1, M=1,ϕ1, ϕ2, ϕ3=0.005, 0.01, 0.03. k=0.5, k_f=0.613, k_{nf}=1.08, Pr=6.2,**B***=1, *Ec*=1, Nr=1

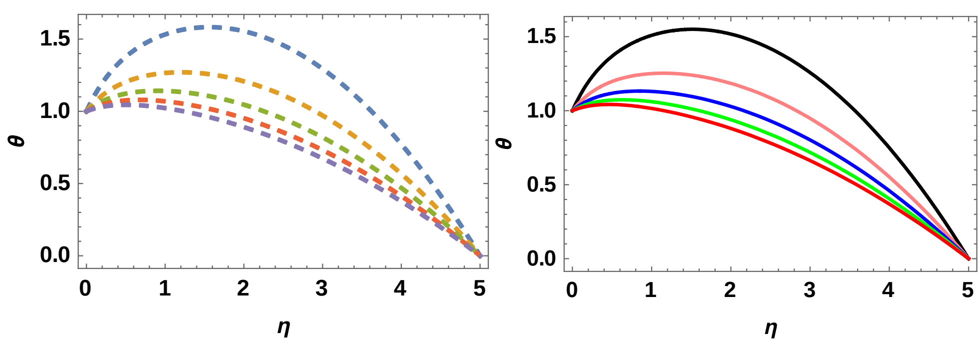

Graph 12 (A & B) Temperature profile $\theta(\eta)$ for various values of Nr, $\boldsymbol{\gamma}$ =1, M=1,ϕ1, ϕ2, ϕ3=0.005, 0.01, 0.03. k=0.5, k_f=0.613, k_{nf}=1.08, Pr=6.2, **B***=1, *Ec*=1

Graph 12 shows that the skin friction coefficient grows as the volume proportion of nanoparticles volume fraction ϕ increases, although the local Nusselt number in graphs 13-14 does not show similar results for increasing Pr value.

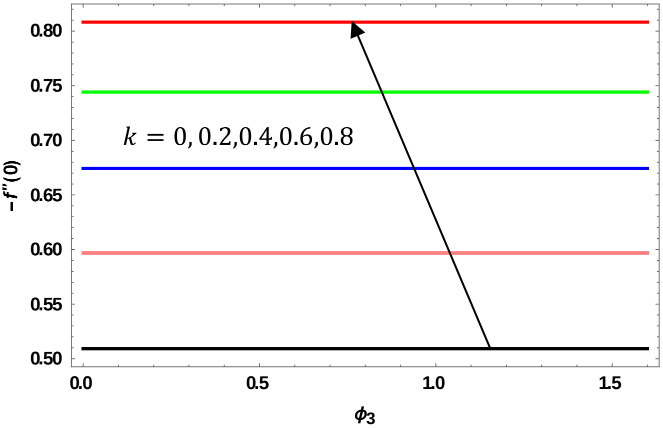

Graph 13. For different levels of the porosity parameter k, skin friction -f''(η) with nanoparticle volume fraction ϕ3

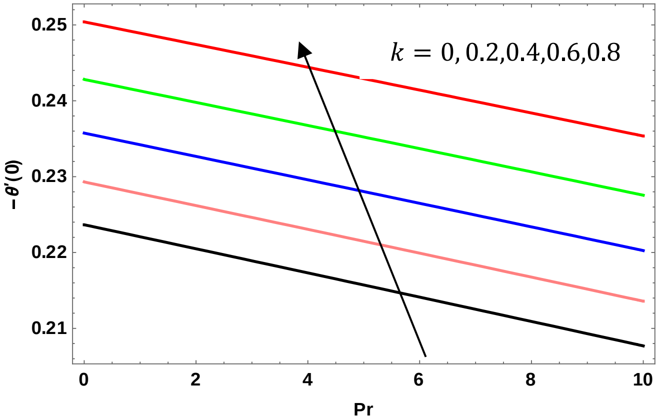

Graph 14. Variations in the Prandtl number Pr and the heat transfer coefficient –θ'(0) for various values of the porosity parameter k

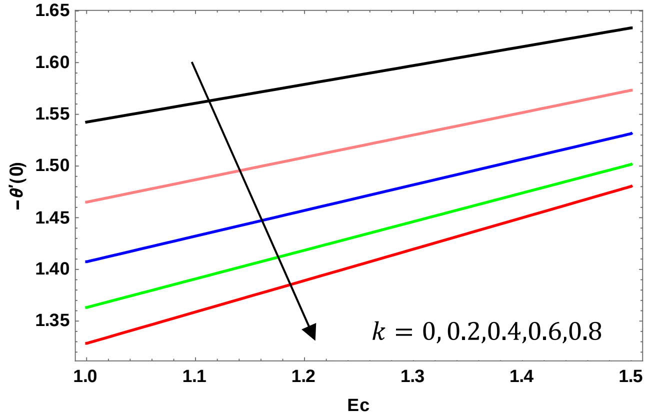

Graph 15. Variation in the Eckert number Ec and the heat transfer coefficient –θ'(0) for different values of the porosity parameter k.

5. Conclusion

We have analysed the 3-dimensional Casson nanofluid flow behavior of momentum and heat transmission across stretched sheet having non-uniform source of heat and heat sink. Graphs are used to describe and display a number of non-dimensional controlling characteristics that affect velocity distribution and heat transfer rate. From the outcomes, we may infer the following. The velocity profiles progressively decrease as the Casson nanofluid parameter raises.

- Local skin friction coefficients in both directions increase numerically when porosity parameter k increases.
- The temperature rises when the Eckert number is taken into account.
- The formation of the temperature profile is aided by the existence of non-uniform heat sources and sinks.
- As thermal radiation parameter Nr rises, the thermal boundary layer and heat thickness rise.

References

1. A. Al-Mamun, S.M. Arifuzzaman, S. Reza-E-Rabbi; Numerical simulation of periodic MHD casson nanofluid flow through porous stretching sheet, *SN Appl. Sci.* 3 (2021) , 271. https://doi.org/10.1007/s42452-021-04140-3.
2. S. Ayesha and B. Shankar; MHD Flow and Heat Transfer of Casson Nanofluid through a Porous Media over a Stretching Sheet, DOI: 10.5772/intechopen.83732.
3. A. Bagh, N. Yufeng, H. Sajjad, M. Abdul, T. Muhammad; Unsteady magneto-hydrodynamic transport of rotating Maxwell nanofluid flow on a stretching sheet with Cattaneo–Christov double diffusion and activation energy, *Thermal Science and Engineering Progress*, 20 (2020), 100720, ISSN 2451-9049.
4. A. Bagh, S. Imran, A. Ali, S. Norazak, A. Liaqat, H. Amir; Significance of Lorentz and Coriolis forces on dynamics of water based silver tiny particles via finite element simulation, *Ain Shams Engineering Journal*, 13(2) (2022), 101572, ISSN 2090-4479.
5. M. Ferdows, A. Jahangir, M. Murtaza, E. Tzirtzilakis; Application of Biomagnetic Fluid Dynamics modeling for simulation of flow with magnetic particles and variable fluid properties over a stretching cylinder, *Mathematics and Computers in Simulation*, 199 (2022), 438-462, ISSN 0378-4754.
6. S.S. Ghadikolaei, K. Hosseinzadeh, D.D. Ganji, B. Jafari; Nonlinear thermal radiation effect on magneto Casson nanofluid flow with Joule heating effect

over an inclined porous stretching sheet, *Case Studies in Thermal Engineering*, 12 (2018), 176-187, ISSN 2214-157X.

7. R. Gnaneswara, M. Ahmed, W. Abbas; Modeling of MHD fluid flow over an unsteady stretching sheet with thermal radiation, variable fluid properties and heat flux, *Mathematics and Computers in Simulation*, 185 (2021), 583-593, ISSN 0378-4754.
8. A. Hamzeh; Numerical Solution of Heat Transfer Flow of Casson Hybrid Nanofluid over Vertical Stretching Sheet with Magnetic Field Effect, *CFD Letters*, 14 (2022), 39-52. 10.37934/cfdl.14.3.3952.
9. N. Ibrar, M.G. Reddy, S.A. Shehzad; Interaction of single and multi-walls carbon nanotubes in magnetized-nano Casson fluid over radiated horizontal needle, *SN Appl. Sci.*, 2 (2020), 677. https://doi.org/10.1007/s42452-020-2523-8
10. A. Kamran, S. Hussain, M. Sagheer, N. Akmal; A numerical study of magnetohydrodynamics flow in Casson nanofluid combined with Joule heating and slip boundary conditions, *Results in Physics*, 7 ,(2017), 3037-3048, ISSN 2211-3797.
11. W. Kouz, W. Owhaib; Numerical analysis of Casson nanofluid three-dimensional flow over a rotating frame exposed to a prescribed heat flux with viscous heating. *Sci Rep*, 12 (2022), 4256.

    https://doi.org/10.1038/s41598-022-08211-2
12. A. Liaquat, O. Zurni, R. Jawad, K. Ilyas, M. El-Sayed; Effects of Stefan Blowing and Slip Conditions onUnsteady MHD Casson Nanofluid Flow Over an Unsteady Shrinking Sheet, *Dual Solutions, Symmetry*, 12 (2020), 487; doi:10.3390/sym12030487
13. S. M. Mani, M. Swati; Some aspects of flow over a non-isothermal unsteady stretched exterior fixed in porous medium among heat production/ amalgamation, *Forces in Mechanics*, 9 (2022), 100142, ISSN 2666-3597.
14. R. Meenakumari, P. Lakshminarayana, K. Vajravelu; Unsteady MHD Flow of a Williamson Nanofluid on a Permeable Stretching Surface with Radiation and Chemical Reaction Effects, *Eur. Phys. J. Special Topics*, 230 (2021), 1355-1370.
15. R. Mohamed, S. Ahmed, A. Aly, A. Chamkha, M. Soliman; MHD Casson Nanofluid Flow Over A Stretching Surface Embedded In A Porous Medium: Effects Of Thermal Radiation And Slip Conditions, *Latin American Applied Research*, 51(4) (2021), 229-239.
16. S. Muradi, A. Liaqat, L. Bagh. Xiaomin, A. Shehzad; Analysis of bio-convective MHD Blasius and Sakiadis flow with Cattaneo-Christov heat flux model and chemical reaction, *Chinese Journal of Physics*, 77 (2022), 1963-1975, ISSN 0577-9073.

17. P.G. Partha, K. Shailendra, M. Susanta; Two layer thin film flow over a stretching sheet with uniform transverse magnetic field, *Journal of Magnetism and Magnetic Materials*, 565 (2023), 170204, ISSN 0304-8853.
18. M. Radha, W. Sridhar, P. Nagesh; Numerical investigations of MHD Casson nanofluid flow over a wedge through porous medium, *AIP Conference Proceedings*, 2375 (2021), 030011.

    https://doi.org/10.1063/5.0066944
19. K. Rafique, M. Imran, M. Misiran, I. Khan, S. Alharbi, P. Thounthong, K. Nisar; Numerical Solution of Casson Nanofluid Flow Over a Non-linear Inclined Surface WithSoret and Dufour Effects by Keller-Box Method, *Frontiers in Physics*, (2019). DOI: 7.10.3389/fphy.2019.00139.
20. A.C.V. Ramudu, K.K. Anantha, V. Sugunamma, N. Sandeep; Influence of Suction/Injection on MHD Casson Fluid Flow over a Vertical Stretching Surface, *J. Therm.. Anal. Calorim.*, 139 (2020), 3675-3682.
21. S.R.R. Reddy, P. Bala Anki Reddy; Thermal radiation effect on unsteady three-dimensional MHD flow of micropolar fluid over a horizontal surface of a parabola of revolution, *Propulsion and Power Research*, 11(1) (2022), 129-142, ISSN 2212-540X.
22. R. Shiva, D. Paramananda; A numerical solution using EFDM for unsteady MHD radiative Casson nanofluid flow over a porous stretching sheet with stability analysis, *Heat Transfer*, (2022), 8020-8042.
23. D. Sudip, M. Swati; MHD nanofluid flow over an absorbent plate in the company of chemical response and zero nanoparticle flux, *Forces in Mechanics*, 7 (2022), 100102, ISSN 2666-3597.
24. S. Thadakamalla, B. Shankar; Effect of inclined magnetic field on flow, heat and mass transfer of Williamson nanofluid over a stretching sheet, *Case Studies in Thermal Engineering*, 23 (2021), 100819, ISSN 2214-157X.
25. R. Vinodkumar, L. Pallavarapu; MHD radiative flow of Williamson nanofluid with Cattaneo-Christof model over a stretching sheet through a porous medium in the presence of chemical reaction and suction/ injection, *Journal of Porous Media*, 25(12) 2022, 1-15.

    DOI: 10.1615/JPorMedia.2022041423.